

Anisotropic diffusion in square lattice potentials: giant enhancement and control

DAVID SPEER¹, RALF EICHHORN² and PETER REIMANN¹

¹ *Universität Bielefeld, Fakultät für Physik, 33615 Bielefeld, Germany*

² *NORDITA, Roslagstullsbacken 23, 10691 Stockholm, Sweden*

PACS 05.45.-a – Nonlinear Dynamics and nonlinear dynamical systems

PACS 05.40.-a – Fluctuation phenomena, random processes, noise, and Brownian motion

PACS 05.60.-k – Transport processes

Abstract – The unbiased thermal diffusion of an overdamped Brownian particle in a square lattice potential is considered in the presence of an externally applied ac driving. The resulting diffusion matrix exhibits two orthogonal eigenvectors with eigenvalues $D_1 > D_2 > 0$, indicating anisotropic diffusion along a “fast” and a “slow principal axis”. For sufficiently small temperatures, D_1 may become arbitrarily large and at the same time D_2 arbitrarily small. The principal diffusion axis can be made to point into (almost) any direction by varying either the driving amplitude or the coupling of the particle to the potential, without changing any other property of the system or the driving.

Introduction. – Thermal diffusion plays a key role in many physical, chemical, and biological processes. At thermal equilibrium, the free diffusion as considered, e.g., by Einstein [1], is generically reduced by an additional periodic potential [2], and – at least for the most common periodic lattice structures – remains spatially isotropic (see below). Out of equilibrium, the main focus has so far been on periodic potentials in one-dimension, perturbed by either a static “bias force” (tilted washboard potentials) [3–5] or by an unbiased, time-dependent driving [6]. The most remarkable finding in both cases is that the diffusion coefficient D may exhibit a giant enhancement over the free (Einsteinian) diffusion coefficient D_0 . More precisely, for asymptotically small D_0 , the ratio D/D_0 diverges, while D itself still tends to zero, apart from certain fine-tuned (non-analytical) potential shapes and system parameters, for which D may remain finite.

Another topic of considerable recent interest concerns the effect of disorder (random deviations from a strictly periodic potential), which may give rise to a further diffusion enhancement or even to anomalous diffusion [7].

Works on genuine new phenomena in higher dimensions are scarce: Guantes and Miret-Artés [8] studied biased diffusion induced by an asymmetric external driving. Sancho et al. and Lacasta et al. [9] put their main focus on (possibly transient) anomalous diffusion effects. Experimentally, Tierno et al. observed giant transversal diffusion of

paramagnetic particles on an uniaxial garnet film in the presence of an oscillating magnetic field [10].

Here, we reconsider the prototypical situation of Brownian motion in a more than one-dimensional periodic potential and we demonstrate that a simple ac driving generically results in anisotropic diffusion, whose direction and magnitude depend in a quite intriguing way on the potential, the driving, and the particle properties.

Model. – To keep things as simple as possible, we specifically focus on a square lattice in two-dimensions and on a square-wave (rectangular) driving. Yet, our main results readily carry over to various other drivings and more general lattice potentials in two as well as in three dimensions.

Our starting point is the the Langevin dynamics

$$M\ddot{\vec{r}}(t) + \eta\dot{\vec{r}}(t) = -\vec{\nabla}U(\vec{r}(t)) + \vec{F}(t) + \sqrt{2\eta kT}\vec{\xi}(t) , \quad (1)$$

where M is the mass of the Brownian particle, η its friction coefficient, and $\vec{r} = x\vec{e}_x + y\vec{e}_y$ its position in the x - y -plane, with \vec{e}_x and \vec{e}_y being the unit vectors in x - and y -direction. Further, $U(\vec{r})$ stands for the spatially periodic potential, $\vec{\nabla}U(\vec{r})$ its gradient, and $\vec{F}(t)$ the temporally periodic force. The last term in (1) accounts for thermal noise as usual [2–4, 6, 8, 9]: T is the temperature, k Boltzmann’s constant, and $\vec{\xi}(t) = \xi_x(t)\vec{e}_x + \xi_y(t)\vec{e}_y$ consists of two independent, delta-correlated, Gaussian noises $\xi_x(t)$,

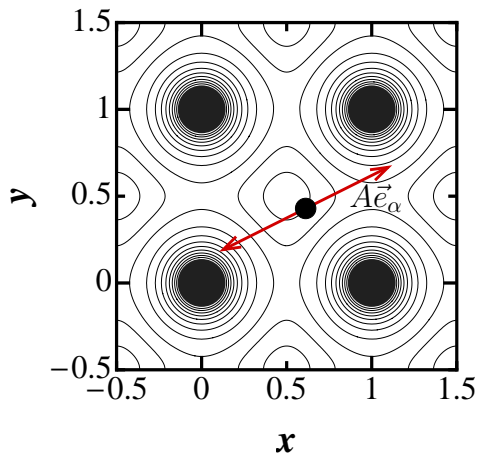


Fig. 1: Schematic illustration of the periodic potential from (2), (3) (black contour lines) and of the square-wave driving from (4) (red double-arrow) which act on the Brownian particle according to (1) (black dot). The depicted choice of parameters $L = 1$, $Q = 1$, and $\alpha = 35^\circ$ represents our “standard example” in eqs. (5), (6) and in figs. 2 - 7. One of the periodic potential minima is located at the center of the plot.

$\xi_y(t)$.

As announced, we specifically address the case that the periodic potential $U(\vec{r})$ is composed of rotation-symmetric on-site potentials $U_1(\vec{r})$ on a square lattice with period L ,

$$U(\vec{r}) = \sum_{m,n=-\infty}^{\infty} U_1(\vec{r} - [m\vec{e}_x + n\vec{e}_y]L). \quad (2)$$

As illustrated by fig. 1, our standard example will be the Yukawa potential

$$U_1(\vec{r}) = Q \exp\{-|\vec{r}|/4L\}/|\vec{r}|, \quad (3)$$

where $Q \geq 0$ quantifies the coupling of the particle to the potential (e.g. the particle charge in the case of a screened electrostatic potential).

Likewise, the announced square-wave driving is formally given by

$$\vec{F}(t) = \vec{e}_\alpha A \text{sign}[\sin(\omega t)] \quad (4)$$

with amplitude A , frequency ω , and direction $\vec{e}_\alpha := \vec{e}_x \cos \alpha + \vec{e}_y \sin \alpha$. In other words, it switches between A and $-A$ every half-period π/ω , and α represents the angle between the driving force and the x -axis, see fig. 1.

Yet, as already said, our main qualitative findings turn out to be largely independent of the above particular choice of on-site potential, lattice structure, and driving.

To further reduce the number of model parameters, we can and will choose the units of length, time, energy, and temperature so that

$$L = 1, \quad \omega = 1, \quad \eta = 1, \quad k = 1, \quad (5)$$

and we focus on the simplest and most important case [2-4,6] that inertia effects are negligible (overdamped limit),

i.e. $M \rightarrow 0$ in (1), yielding

$$\dot{\vec{r}}(t) = -\vec{\nabla}U(\vec{r}(t)) + \vec{F}(t) + \sqrt{2T}\vec{\xi}(t). \quad (6)$$

We remark that in the presence of an additional, externally applied static bias force, a quite interesting response behavior in the form of a directed net particle motion arises [11,12]. In the following, our main focus will be on a quite different issue, namely the unbiased diffusion of a Brownian particle in the absence of any further perturbation.

Diffusion matrix. – For symmetry reasons, the above specified dynamics rules out any systematic particle transport, i.e. we are dealing with a purely diffusive, unbiased Brownian motion, characterized by a 2×2 diffusion matrix \mathbf{D} with matrix elements

$$D_{ij} = \lim_{t \rightarrow \infty} \frac{\langle r_i(t) r_j(t) \rangle}{2t}, \quad (7)$$

where $r_i, r_j \in \{x, y\}$ (see below (1)) and where $\langle \cdot \rangle$ indicates the ensemble average over many realizations of the stochastic dynamics. For ergodicity reasons and due to the long-time limit in (7), the initial conditions are irrelevant and we can without loss of generality focus on

$$\vec{r}(0) = \vec{0}. \quad (8)$$

Since \mathbf{D} is symmetric and positive, there are two orthogonal eigenvectors with eigenvalues

$$D_1 \geq D_2 > 0. \quad (9)$$

Essentially, a statistical ensemble of (non-interacting) Brownian particles, all starting from the origin at time $t = 0$, thus evolves in the course of time into a bigger and bigger “particle cloud” of ellipsoidal shape, see fig. 2. For large times t , and neglecting local details on the scale of the spatial period L , this cloud is quantified by a Gaussian probability density [4,13] of variance $2D_1 t$ along some “fast principal axis” $\vec{e}_\Theta := \vec{e}_x \cos \Theta + \vec{e}_y \sin \Theta$, and of variance $2D_2 t$ along the orthogonal “slow principal axis”. The angle Θ between “fast direction” and x -axis is thus 180° -periodic, i.e.

$$\Theta \text{ and } \Theta + 180^\circ \text{ are equivalent.} \quad (10)$$

Free diffusion (vanishing $U(\vec{r})$ and $\vec{F}(t)$) according to Einstein [1] amounts to $D_1 = D_2 = D_0$ with $D_0 = kT/\eta$ for the original dynamics (1) and $D_0 = T$ for the rescaled dynamics (6).

Including the periodic potential $U(\vec{r})$, but still without oscillating force $\vec{F}(t)$, the system (2)-(6) is still invariant under rotations by 90° , implying isotropic diffusion ($D_1 = D_2$).

Including also the driving $\vec{F}(t)$, this symmetry is broken, implying anisotropic diffusion ($D_1 > D_2$) in the generic case. The remaining two symmetry arguments are: (i) It

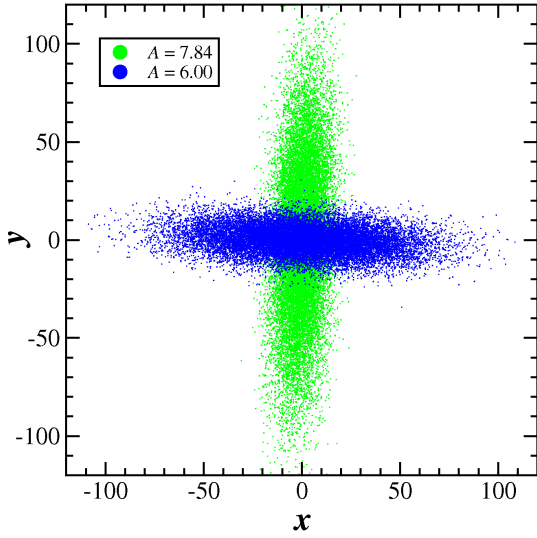


Fig. 2: Typical examples of diffusive “particle clouds”. The corresponding (unbiased) Gaussian probability densities are completely characterized by the variance $2D_1t$ along the long principal axis and by the variance $2D_2t$ along the short principal axis of the ellipsoidal clouds. In other words, the plot must simply be rescaled by \sqrt{t} in the course of time. Quantitatively, every single depicted point represents a numerical solution at time $t = 10^5$ of the stochastic dynamics (2)-(6) with initial condition (8) and parameters $Q = 1$, $\alpha = 35^\circ$, $T = 5 \cdot 10^{-5}$, and $A = 6$ (blue), $A = 7.84$ (green).

is sufficient to consider $\alpha \in [0^\circ, 45^\circ]$. (ii) If the driving direction \vec{e}_α coincides with a symmetry axis of the square lattice (i.e. $\alpha = 0^\circ$ or $\alpha = 45^\circ$) then \vec{e}_Θ will be parallel or orthogonal to \vec{e}_α . In any other case ($0^\circ < \alpha < 45^\circ$) it is impossible to predict \vec{e}_Θ a priori.

After a couple of unsuccessful attempts one furthermore realizes that analytical progress is quite hopeless. Therefore we now turn to the presentation of our numerical results (next Section), followed by a brief account of the underlying basic physical mechanisms (Section ‘Discussion’).

Results. – We first exemplify the most interesting regime of the parameters Q , A , α and later provide a more systematic exploration: fig. 3 depicts the “fast” and “slow” diffusion coefficients D_1 and D_2 together with their ratio D_1/D_2 and the “fast direction” Θ . A pronounced anisotropy of the diffusion is indicated by the fact that $D_1 \gg D_2$. The corresponding “particle cloud” (see fig. 2 and below eq. (9)) thus actually resembles a very narrow “particle beam”. Its orientation Θ may assume any value between 0° and (almost) -180° upon variation of the driving amplitude A for the specific choice of the remaining parameters used in fig. 3. For other such choices, an even larger range of Θ -values can be covered. Since Θ and $\Theta + 180^\circ$ are equivalent (see (10)), we can conclude that essentially any possible orientation of the “fast” diffusion direction can be realized upon variation of A , without changing any other property of the system or the driving, see fig. 2.

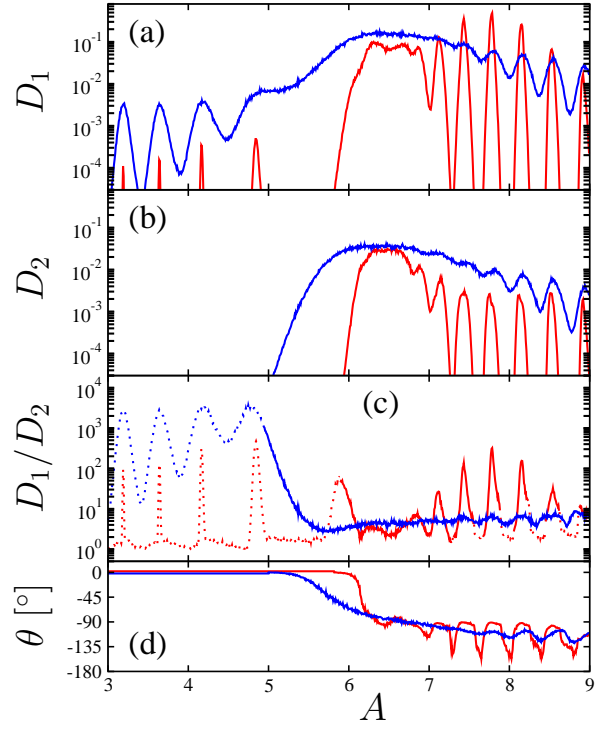


Fig. 3: Eigenvalues $D_{1,2}$ of the diffusion matrix (7) and angle Θ between first eigenvector and x -axis (see also (9,10)) versus driving amplitude A , obtained – similarly as in fig. 2 – from 800 numerical realizations over 10^5 time units of the stochastic dynamics (2)-(6) with initial condition (8) and parameters $Q = 1$, $\alpha = 35^\circ$, and $T = 5 \cdot 10^{-4}$ (blue), $T = 5 \cdot 10^{-5}$ (red). In spite of the very large final time $t = 10^5$, the average particle displacement along the “slow principal axis” (and possibly also along the “fast” one) was less than one spatial period $L = 1$ for some A -values. The corresponding D_2 (and D_1) values are below the range depicted in (b) and (a). In (c), the corresponding results are marked by dotting the curves. They do not represent the “true” limits in (7), since $t = 10^5$ is still too small. On the other hand, sufficiently large t -values are way beyond our numerical capabilities. In (d) we did not dot the corresponding A regions since we are quite confident that the depicted results are already very close to the “true” long time limit.

Decreasing the temperature T yields larger D_1/D_2 ratios for practically all amplitudes A in fig. 3 for which the long time limit in (7) could be numerically reached, i.e. the diffusion anisotropy gets more pronounced. Whereas D_2 always decreases upon lowering the temperature, D_1 increases within certain “ A -windows” around $A = 7.4$, $A = 7.8$, $A = 8.2$ etc., and decreases otherwise.

According to fig. 4, analogous findings are recovered upon variation of the potential strength Q from (3). Hence, particles with different “charges” Q can be diffusively “beamed” into different directions very “fast” and with very high precision. In other words, a periodic “surface potential” can act as a very efficient particle sorting device.

A more detailed low-temperature asymptotics of D_i ($i =$

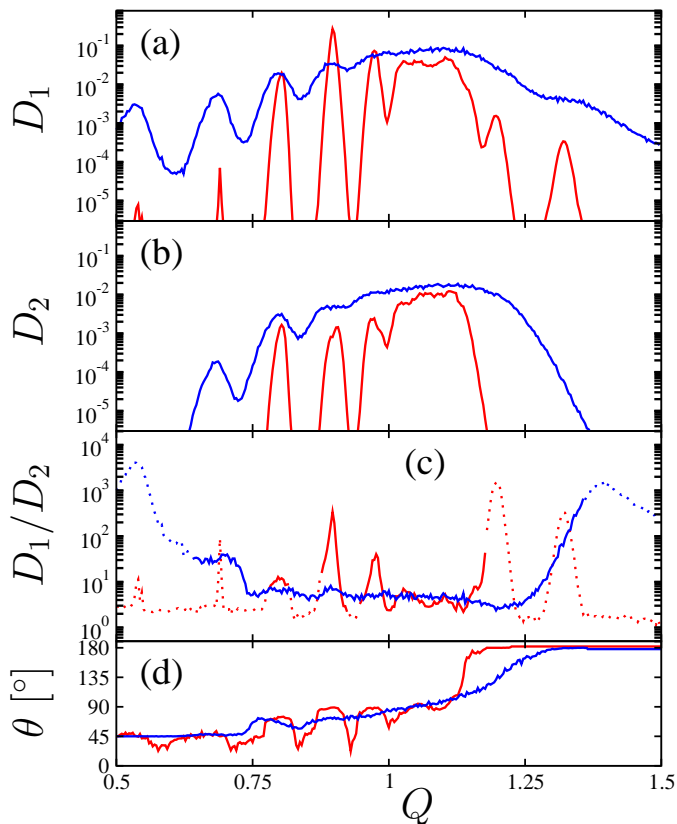


Fig. 4: Same as fig. 3 but for varying coupling strength Q and fixed driving amplitude $A = 7$.

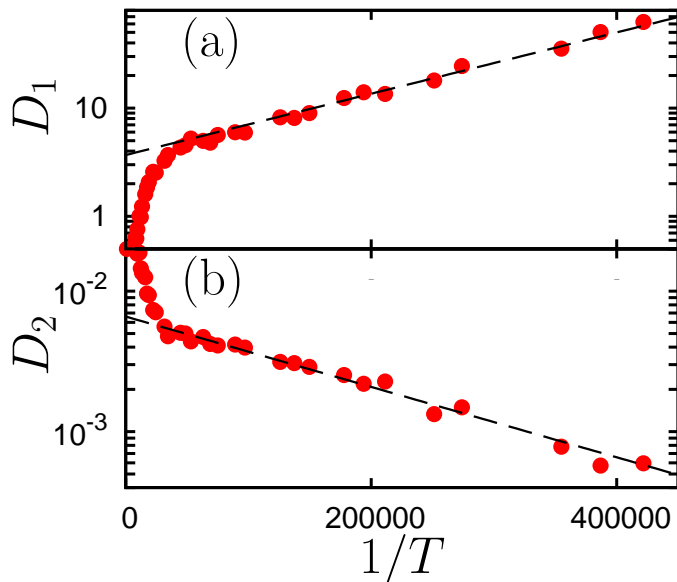


Fig. 5: Eigenvalues $D_{1,2}$ of the diffusion matrix (7), presented as Arrhenius-plot ($\log D_i$ versus $1/\text{temperature}$), from 1000 numerical realizations over 10^5 time units of the stochastic dynamics (2)-(6) with initial condition (8) and parameters $Q = 1$, $\alpha = 35^\circ$, and $A = 7.77$. Dashed: Asymptotic eq. (11).

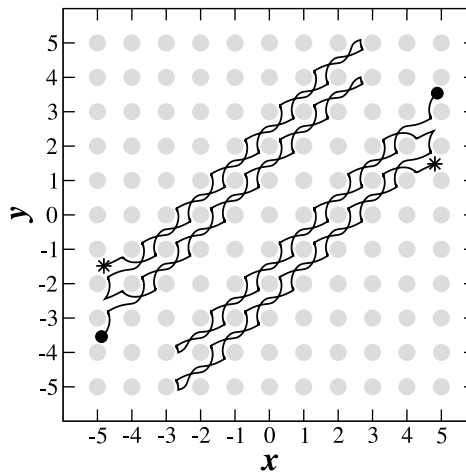


Fig. 6: A pair of transporting attractors, arising due to spontaneous symmetry breaking. Each of the two black trajectories represents a solution of the deterministic dynamics (2)-(6) with $Q = 1$, $A = 7$, $\alpha = 35^\circ$, and $T = 0$. The “star” of the lower right trajectory indicates the initial position at $t = \pi$ and the “dot” the final positions at $t = 5\pi$, i.e. after 2 temporal periods of the square-wave driving (4). At the end of the depicted evolution, the solution has advanced along the y axis by exactly two spatial periods of the periodic potential (indicated by the grey dots, see also fig. 1). In other words, we are dealing with a periodic attractor with $v = 1$ and $\phi = 90^\circ$. Likewise, the upper left trajectory advances between $t = 0$ and $t = 4\pi$ into the opposite direction.

1, 2) is provided by fig. 5, evidencing an Arrhenius-type behavior

$$D_i \sim \exp\{-E_i/T\} \quad (11)$$

with certain “effective energies” $E_1 < 0 < E_2$. The same behavior is recovered within all of the above mentioned “ A -windows”. For all other A -values, one finds (as expected and hence not shown) the same asymptotics as in (11), but now with $0 < E_1 < E_2$.

We thus can conclude that the diffusive particle motion can become arbitrarily “fast” and anisotropic for sufficiently small temperatures T . Likewise, in comparison to the free diffusion coefficient $D_0 = T$, the ratio D_1/D_0 diverges and D_2/D_0 approaches zero for asymptotically small T .

Discussion. – For an intuitive understanding of what is going on, we first focus on the dynamics (2)-(6) in the deterministic limit ($T = 0$). Without driving ($A = 0$) the particle readily settles down into one of the local minima of the periodic potential (2), (3), see also fig. 1. Upon increasing A , all those point attractors evolve via a complicated sequence of bifurcations into (possibly coexisting) periodic, quasi-periodic, or chaotic attractors, whose quite intricate details also depend on the values of Q and α [11, 12]. As might not have been immediately anticipated, but in fact is rather plausible at second glance, some of the so emerging deterministic attractors give rise to a permanent directed particle motion, see fig. 6. For symmetry

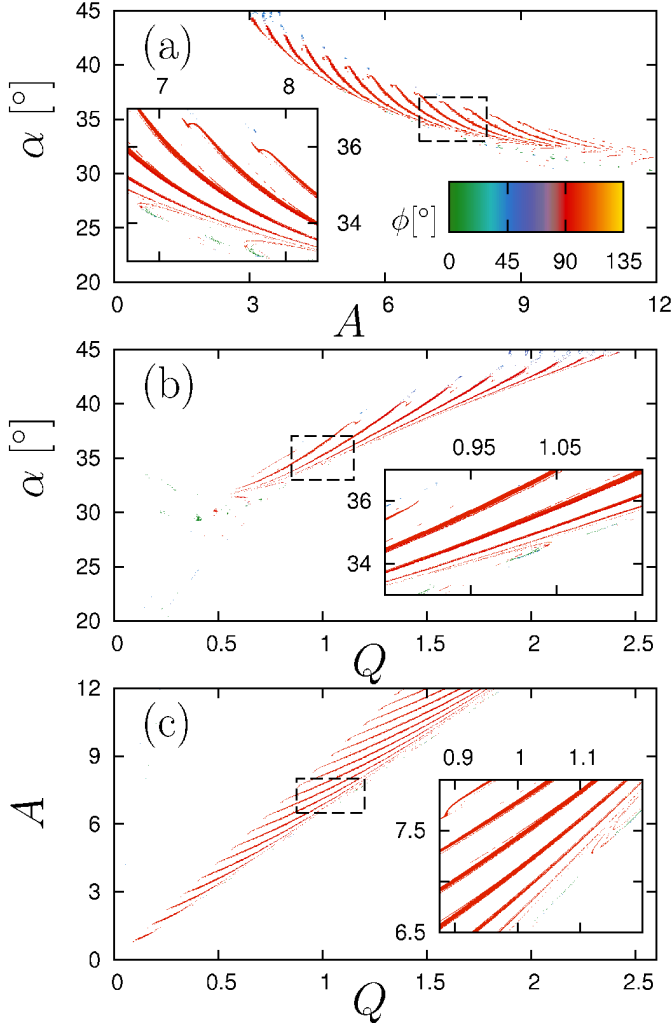


Fig. 7: Deterministic attractors by solving (2)-(6) with $T = 0$ numerically for a large number of randomly sampled initial conditions $\vec{r}(0)$. (a) Varying driving angle α and amplitude A at fixed coupling strength $Q = 1$. (b) Varying α and Q at fixed $A = 7$. (c) Varying A and Q at fixed $\alpha = 35^\circ$. White: All numerically detected attractors are non-transporting (vanishing net velocity $\vec{v} = \lim_{t \rightarrow \infty} \vec{r}(t)/t$). Colored: There is a symmetric pair of attractors exhibiting spontaneous transport of opposite velocities (cf. fig. 6). The angle ϕ between these velocities and the x -axis is indicated by the different colors. The overwhelming majority of the colored pixels corresponds to $\phi = 90^\circ$ (red), but also a few blue and green pixels are still discernible. In most cases, the modulus of the velocities $|\vec{v}|$ was found to be of order one (not shown). Insets: Magnification of dashed rectangles.

reasons, such “transporting attractors” always appear in pairs with opposite transport velocities by way of spontaneous symmetry breaking. Besides such a pair, there may or may not coexist additional (transporting or non-transporting) attractors. The actual occurrence of those transporting attractors and the concomitant quantitative transport velocities \vec{v} are only accessible by numerical means: fig. 7 depicts such numerical results for three rep-

resentative cross sections through the full, 3-dimensional α - A - Q parameter space.

Turning to small but finite temperatures T , the above deterministic attractors become metastable states since the thermal noise now induces rare transitions between them. For weak to moderate driving amplitudes A , these are mainly “hopping” transitions between neighboring potential wells in x - and y -direction (cf. fig. 1) at certain rates γ_x and γ_y , respectively. Since the driving $\vec{F}(t)$ predominantly acts along the x -direction for $0 < \alpha < 45^\circ$, it seems plausible that $\gamma_x > \gamma_y$. Hence one can infer that

$$D_1 \approx L^2 \gamma_x / 2, \quad (12)$$

$$D_2 \approx L^2 \gamma_y / 2. \quad (13)$$

Therefore, we can conclude that $\Theta \approx 0^\circ$. From the usual Boltzmann-Arrhenius temperature dependence of the rates $\gamma_{x,y}$ one finally recovers (11) with $0 < E_1 < E_2$. For the rest, the rates $\gamma_{x,y}$ and hence $D_{1,2}$ from (12,13) may still depend on A (and likewise on Q and α) in a very complicated way. Altogether, these considerations explain the main features of fig. 1 up to about $A = 6$.

Next we focus on the “red stripes” in fig. 7, indicating two symmetric attractors with spontaneous transport in y -direction at certain velocities $\pm v$. Denoting by γ_y the rate of noise induced transitions between them, a similar calculation as in Ref. [5,14] yields for the diffusion coefficient in y -direction the approximation

$$D_1 \approx v^2 / (2\gamma_y), \quad (14)$$

whereas in x -direction one obtains similarly as in (12) the approximation

$$D_2 \approx L^2 \gamma_x / 2. \quad (15)$$

Hence, one can conclude that $\Theta \approx \pm 90^\circ$. This provides an explanation of eq. (11) with $E_1 < 0 < E_2$, an explanation of fig. 3 within the above mentioned “ A -windows”, and an explanation of fig. 5. Moreover, we recognize that these “ A -windows” are in fact the descendants of the “red stripes” in fig. 7.

So far, we tacitly neglected the possibility that besides the transporting attractors there may still coexist further non-transporting attractors. Numerically, one finds that this is indeed the case within a subset of the colored regions in fig. 7 (not shown). In such a case, the noise induced transitions between the various attractors are governed by several different rates, resulting in similar but more complicated estimates for $D_{1,2}$ than in (12)-(15).

Analogous generalizations apply for the small parameter regions in fig. 7 which are colored differently from red, corresponding to a spontaneous deterministic transport into a direction substantially different from $\phi = 90^\circ$.

Coming back to the remaining A -values in fig. 3 – namely those larger than about $A = 6$ but not contained in one of the A -windows – it turns out that, essentially, again thermal hopping prevails, but now predominantly in

steps of $\sqrt{2}L$ along the bisectrix $y = x$, hence $\Theta \approx -135^\circ$. Occasionally, one also encounters more complicated types of motion, resulting in even smaller Θ -values.

As expected, with increasing temperature T , all these features become more and more “washed out” in fig. 3. Especially, this applies to the neighborhood of $A = 6.5$, in accordance with the tightly nested red and white stripes in the corresponding region of fig. 7.

Analogous considerations apply to fig. 4. Overall, we thus can conclude that for sufficiently low temperatures T , giant anisotropic diffusion arises within all colored parameter regions in fig. 7, and that pronounced variations of the principal diffusion axes are expected whenever crossing a border between colored and white regions.

The entire pertinent parameter regions in fig. 7 are not very large as far as their measure is concerned, but still very appreciable for instance from the following viewpoint: For (almost) any given amplitude A it is possible to find angles α and coupling strengths Q for which all those effects can be observed [12].

Finally, it also seems worth mentioning that in contrast to giant diffusion enhancement in one-dimensional periodic potentials [3, 6], in our present case (i) not only the ratio D_1/D_0 , but also D_1 itself diverges for asymptotically small temperatures, and (ii) the pertinent parameter regions are of finite measure.

Conclusions. – Starting with Einstein’s ground breaking work on Brownian motion [1], the subject of diffusion has attracted a lot of attention due to its practical relevance in numerous specific systems, but also due to its theoretical interest as a fundamental form of transport per se. Here, we reconsidered diffusion in a particularly simple “minimal model”: a spatially periodic system, driven out of equilibrium in one of the experimentally most natural and common ways, namely by an oscillating driving force. Our first main finding is an extreme anisotropy of the diffusion, whose “speed” in one direction may grow exponentially fast as temperature decreases, while the perpendicular “speed” approaches zero exponentially fast. Our second main finding is that the principal axes of the anisotropic diffusion can be made to point into (practically) any direction by solely varying e.g. the ac driving amplitude or the coupling of the particle to the periodic potential, but without changing any other property of the system or the driving.

The indispensable prerequisites for those diffusion effects are very weak and ubiquitous: Brownian motion in a spatially periodic lattice potential under the action of an oscillating driving force is a paradigmatic scenario in a large variety of different contexts, e.g. diffusion on the surface [8] but also in the bulk of a crystal under the action of electromagnetic perturbations, migration in periodic arrays of laser traps, or in periodically structured micro- or nano-fluidic systems, to name but a few [9, 10, 12].

One reason why those very fundamental diffusion phenomena have not been discovered earlier may be the fact

that the underlying key mechanisms of spontaneous symmetry breaking has not been naturally associated with such systems up to now. A second reason is that a very careful numerical exploration is required with a clear idea of what one is actually looking for. In turn, once the quantitative numerical predictions for a specific experimental system are available, verifying and exploiting the predicted effects seems quite feasible and worth while to us.

This work was supported by Deutsche Forschungsgemeinschaft under SFB 613 and RE1344/5-1

REFERENCES

- [1] EINSTEIN A., *Ann. Phys. (Leipzig)*, **17** (1905) 549.
- [2] LIFSON S. and JACKSON J.L., *J. Chem. Phys.*, **36** (1962) 2410.
- [3] PARRIS P.E., KUS M., DUNLAP D.H. and KENKRE V.M., *Phys. Rev. E*, **56** (1997) 5295; COSTANTINI G. and MARCHESONI F., *Europhys. Lett.*, **48** (1999) 491; REIMANN P. ET AL., *Phys. Rev. Lett.*, **87** (2001) 010602; *Phys. Rev. E*, **65** (2001) 031104; BLICKLE V., SPECK T., SEIFERT and BECHINGER C., *Phys. Rev. E*, **75** (2007) 060101(R); EVSTIGNEEV M. ET AL., *Phys. Rev. E*, **77** (2008) 041107.
- [4] LUBENSKY D.L. and NELSON D.R., *Biophys. J.*, **77** (1999) 1824.
- [5] LINDNER B. and NICOLA E.M., *Phys. Rev. Lett.*, **101** (2008) 190603.
- [6] GANG H. ET AL., *Phys. Rev. Lett.*, **76** (1996) 4874; SCHREIER M. ET AL., *Europhys. Lett.*, **44** (1998) 416; REGUERA D. ET AL., *Europhys. Lett.*, **57** (2002) 644; DUBKOV A.A. and SPAGNOLO B., *Phys. Rev. E*, **72** (2005) 041104; COUPIER G. ET AL., *EPL*, **77** (2007) 6001; BORROMEO M. and MARCHESONI F., *Phys. Rev. E*, **78** (2008) 51125; ROMANCZUK P., MÜLLER F. and SCHIMANSKY-GEIER L., *Phys. Rev. E*, **81** (2010) 061120.
- [7] DERRIDA B., *J. Stat. Phys.*, **31** (1983) 433; BOUCHAUD J.-P. and GEORGES A., *Phys. Rep.*, **195** (1990) 127; HARMS T. and LIPOWSKY R., *Phys. Rev. Lett.*, **79** (1997) 2895; LEE H.S. and AND GRIER D.G., *Phys. Rev. Lett.*, **96** (2006) 190601; REIMANN P. and EICHHORN R., *Phys. Rev. Lett.*, **101** (2008) 180601; SIEGLE P., GOYCHUK I. and HÄNGGI P., *Phys. Rev. Lett.*, **105** (2010) 100602; KHOURY M., LACASTA A.M., SANCHO J.M. and LINDENBERG K., *Phys. Rev. Lett.*, **106** (2011) 090602.
- [8] GUANTES R. and MIRET-ARTÉS S., *Phys. Rev. E*, **67** (2003) 046212.
- [9] SANCHO J.M. ET AL., *Phys. Rev. Lett.*, **92** (2004) 250601; LACASTA A.M. ET AL., *Phys. Rev. E*, **70** (2004) 051104.
- [10] TIerno P. ET AL., *Phys. Rev. Lett.*, **105** (2010) 230602.
- [11] SPEER, D., EICHHORN R. and REIMANN P., *Phys. Rev. Lett.*, **102** (2009) 124101.
- [12] SPEER D., *PhD-Thesis, Chapter 4* (Bielefeld 2011, <http://bieson.ub.uni-bielefeld.de/volltexte/2011/1848/>).
- [13] RISKEN H., *The Fokker-Planck Equation* (Springer-Verlag, Berlin) 1984.

- [14] SCHELL M., FRASER S. and KAPRAL R., *Phys. Rev. A*, **26** (1982) 504; REIMANN P. and VAN DEN BROECK C., *Physica D*, **75** (1994) 509.